fluids

MDPI

Article

A Robust Hybrid Staggered/Collocated Mesh Scheme for CFD on Skewed Meshes

Raad Issa [1,*] and Giovanni Giustini [2]

[1] Mechanical Engineering Department, Imperial College London, London SW7 2AZ, UK
[2] Department of Mechanical and Aerospace Engineering, University of Manchester, Manchester M13 9PL, UK; giovanni.giustini@manchester.ac.uk
* Correspondence: r.issa@imperial.ac.uk

Abstract

In this study, a finite-volume computational fluid dynamics (CFD) technique for application on skewed meshes using staggered pressure nodes is proposed. The method is based on the derivation of a momentum equation for the cell face velocities from appropriately discretised momentum equations in the two cells surrounding the cell face with the driving pressure difference pertaining to the staggered adjacent nodes. In this way, a staggered mesh-like method is obtained that would prevent the occurrence of oscillatory behaviour in pressure or velocity fields. The cell-face velocities are then forced to obey continuity via an equation for pressure akin to other standard CFD schemes. This article describes the formulation of the cell-face momentum equation as well as the way the nodal velocity is reconstructed from the surrounding cell-face velocities. The method is demonstrated to recover the advantages of the PISO solution algorithm that were diminished in implementations in collocated schemes. It is also validated on a reference two-dimensional, steady viscous flow case on both rectangular and skewed meshes to verify its accuracy. It is then applied to the case of an unsteady vortex-shedding flow past a square obstacle, on both rectangular and skewed meshes, and the results are compared with a solution obtained from a collocated method as well as with an experimental value of the Strouhal number.

Keywords: staggered-mesh finite-volume CFD method; skewed meshes; cell-face momentum equation from collocated mesh discretization; reconstruction of nodal velocity from cell-face velocities; validation on inviscid and viscous; validation for steady and unsteady flow; kinetic energy conservation; comparison of performance of method against collocated scheme

1. Introduction

To the present authors' knowledge, the group at the Los Alamos laboratory (e.g., Harlow and Welch [1], amongst others) were the first to introduce the staggered mesh methodology to suppress the pressure–velocity decoupling that manifests itself in oscillatory pressure field encountered in the finite-volume solution of the incompressible fluid flow equation. This technique was rapidly and widely adopted by several workers, most notably in methods based on the work of Patankar and Spalding [2]. Such a technique was implemented on regular orthogonal meshes that are intrinsically limited to simple geometries, and is not well-suited to general skewed and unstructured meshes that are demanded for complex geometries in modern industrial applications. For research purposes, however, especially in investigations of turbulence models or Large Eddy Simulation (LES)

Check for updates

Received: 25 December 2025
Revised: 28 January 2026
Accepted: 11 February 2026
Published: 14 February 2026

Copyright: © 2026 by the authors. Licensee MDPI, Basel, Switzerland. This article is an open access article distributed under the terms and conditions of the Creative Commons Attribution (CC BY) license.

and Direct Numerical Simulation (DNS), regular orthogonal meshes in simple geometries suffice; hence, several research computer codes that are aimed at such applications continue to be based on the staggered mesh arrangement.

Many, if not most, current finite-volume methods use Cartesian velocity components that lead to the most compact form of the governing equations, thereby enabling their simple discretisation on skewed and unstructured meshes. However, mesh stagger had in the past been deemed to be unusable in conjunction with these velocity components, as the velocity directions can become totally misaligned with the mesh orientation. Reversion to collocated meshes had been considered to be the only way forward for dealing with complex meshes, but for the problem of pressure-velocity decoupling. To surmount that problem, Rhie and Chow [3] developed their well-known pressure interpolation formula to suppress the decoupling on collocated meshes. This approach (described by Ferziger and Peric [4]) was soon adopted by many workers and has since become a standard methodology used in mainstream CFD codes, including the main commercially available ones as well as the open-source code OpenFoam.

However, the pressure interpolation scheme in its various forms suffers from several drawbacks, these being as follows:

(i) The interpolation introduces dissipation terms that tend to infringe the principle of conservation of kinetic energy (see, for example, Benhamadouche and Laurence [5] and Jofre et al. [6]).
(ii) When additional forces such as those due to buoyancy and Reynolds stresses (arising from the Reynolds Stress Model of turbulence) are present, the problem of oscillatory pressure field reappears unless special interpolation practices akin to the Rhie and Chow formulation for pressure are used.
(iii) In the presence of large pressure gradients, the computed nodal velocities can display spurious values that are not bounded by the surrounding face velocities.
(iv) The coupling between pressure and velocity is weaker than that with the staggered mesh arrangement, leading to poorer performance in the solution strategy, as exemplified by the application of the PISO method (Issa [7]) shown later in this article.

Of the above deficiencies, the non-conservation of kinetic energy can be a serious impediment to the application of LES and DNS computations where high numerical fidelity is required.

Several efforts have been made in the past to develop schemes for implementing the staggered arrangement on unstructured meshes utilising Cartesian velocity components, examples of which are the works by Perot [8], Perot et al. [9], Vidovic et al. [10], Wenneker et al. [11–13], Wesseling et al. [13], Zijlema et al. [14], Mahesh et al. [15], and Ventosa-Molina et al. [16]. Some of those schemes formulate the discretised momentum equations on hybrid control volumes that are constructed from portions of the actual mesh used or are overlaid over it. Most of those are tailored to tetrahedral meshes only. Implementation has been mainly limited to 2D domains, although an extension to 3D was made by Zhang et al. [17]. Hence, these schemes are perhaps too complicated to implement in a general-purpose CFD code such as that currently employed in industry.

Lately, an approach has been developed to combine standard collocated discretisation with a staggered scheme, e.g., by Ge & Sotiropoulos [18] and Natarajan & Sotiropoulos [19], among others. The scheme presented here falls within such a category. We refer to such schemes as being *hybrid* as they utilise both approaches.

Other authors, such as Aguerre et al. [20], adopted a different approach to recover the strong pressure-velocity coupling, typical of staggered methods, while still using a fully collocated method. The developers of the commercial code FLUENT also tackled the deficiency of a collocated approach in a multiphase application by proposing a procedure

called PRESTO [21] in which the pressure nodes are located at cell faces, thus emulating the staggered approach, but this is recommended only for some multiphase applications.

Hybrid collocated/staggered schemes solve a momentum equation for the cell-face velocity derived from an interpolation of the momentum fluxes pertaining to the surrounding cell-centred governing equations; this is different from standard collocated schemes that use the Rhie & Chow interpolation which is based on interpolating cell-centred pressure gradients and nodal (it should be noted that the term *node* used here denotes cell-centre throughout the article and not vertices as denoted in some publications) velocities to compute the cell face velocities. As with other pressure-based schemes, the hybrid methods enforce continuity on the velocities normal to cell faces. However, while in collocated schemes the nodal velocities are computed from their own momentum equations, here, they are reconstructed (interpolated) directly from the cell face velocities. This reconstruction process appears to have a profound effect on the accuracy of the final solution. Perot [8] proposed what appears to be an elegant derivation for computing the nodal Cartesian components from the velocities normal to cell faces. Natarajan & Sotiropoulos [19] demonstrated that the Perot reconstruction was accurate only on uniform meshes because of its first-order basis and proposed a modification employing a correction based on gradients of the nodal velocities, a feature that is absent from other proposed approaches (such as Weller & Shahrokhi [22]). However, it was pointed out elsewhere in Ref. [19] that the accuracy of their scheme is highly dependent on the way the corrective velocity gradients are computed, a feature that was also found by the present authors on highly skewed meshes, where widely different results were obtained from different gradient calculation schemes. Other workers use polynomials for the Cartesian velocity components to fit the normal cell-face mass fluxes; however, as noted by Jofre et al. [6], that procedure usually leads to over- or under-determined systems, which demand the use of a cumbersome least square technique to solve.

Like the works referred to above, the present article proposes a hybrid collocated/staggered technique based on the formulation of momentum equations for the Cartesian cell-face velocities using interpolation of the discretised momentum equations for the corresponding nodal velocity components in the two cells straddling a cell face. The simplicity of the approach is rooted in its reliance on a single mesh, which can be anything from tetrahedral to fully polyhedral. The technique differs from other existing schemes in two fundamental aspects:

(i) The derivation of the momentum equation for the cell-face velocities incorporating *velocity gradients*;
(ii) The reconstruction of the nodal velocity, which is based here on interpolation from the *Cartesian face velocities* themselves rather than the face-normal velocities/fluxes.

This could make the technique directly applicable to current widely used general-purpose codes (e.g., OpenFOAM) with apparently little effort needed for modification.

Although no formal analysis is offered to prove the scheme order of accuracy, the results presented herein verify by way of application to several 2D cases that it both (i) maintains the order accuracy of the collocated discretisation scheme (second-order centred difference is used here) and (ii) conserves kinetic energy in frictionless flow (at least on a uniform regular mesh). The results also indicate (iii) highly improved robustness of the solution procedure (specifically in conjunction with the PISO algorithm) compared to the collocated mesh technique, thus coping with very large Courant numbers. Comparisons between the performance of the hybrid staggered method and the collocated one are made using exactly the same discretisation schemes both spatially and temporally.

2. Discretisation

2.1. Preamble

Consider an arbitrary polyhedral control volume as shown in Figure 1, with Cartesian components of the velocity vector **u** being stored at the cell centre *0*, where the pressure is also stored. Although the figure is shown in two dimensions, this is done for ease of presentation, and the principles of the method apply to three dimensions. The arrangement is very much like the standard practices employed in collocated methods. The velocity component normal to a cell face f is denoted by q, where

$$q_f = \boldsymbol{u}_f \cdot \mathbf{n}_f \tag{1}$$

and $\mathbf{n}_f$ is the outward unit vector normal to face f.

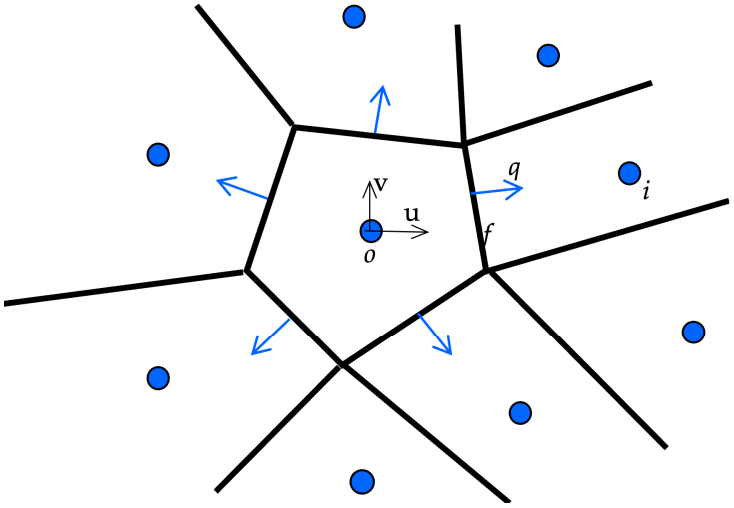


Figure 1. Arbitrary cell with centre at o and cell face f.

In standard collocated methods, the momentum equations are discretised for the Cartesian components of **u** at each node and are then solved. In the presently proposed staggered scheme, the spatial derivatives of **u** are discretised in the same way, but no equations for the components of **u** at nodes are solved. Instead, the face Cartesian velocities are computed using interpolated terms in the momentum equations of the Cartesian components of **u** at the two nodes straddling the corresponding cell-face (nodes o and i in Figure 1); as in any staggered scheme, the pressure gradient acting on $\mathbf{u}_f$ is also obtained from the same straddling nodes. This approach is similar to that introduced by Natarajan & Sotiropoulos [19]. The continuity equation is naturally based on the face normal velocities q. The Cartesian components of the velocity vector **u** at cell centres are then reconstructed from the prevailing Cartesian cell face velocities, and this differs from other works where the reconstruction is based on the face normal velocities. Since the process is applied to individual cell faces, it is, in principle, adaptable directly to multiply connected cells (often called hanging nodes), as depicted in Figure 2, although this is not demonstrated herein.

2.2. The Momentum Equations for the Face Velocities

A discrete form of the momentum equation for the Cartesian and face-normal velocities at a generic cell face f (Figure 3) may now be formulated as if it is made up of portions of the momentum balances at the surrounding control volumes that straddle the cell face. In the figure, $\boldsymbol{d}_{of}$ and $\boldsymbol{d}_{fi}$ are the distance vectors connecting cell centres o and i, respectively, to the centre of the cell face f.

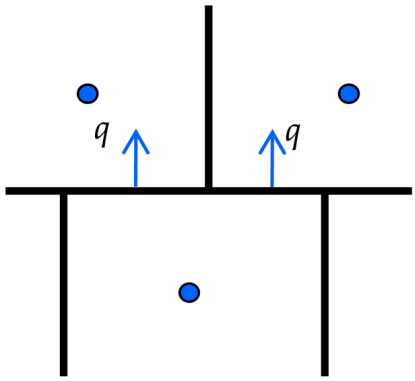


Figure 2. Multiply connected cell faces.

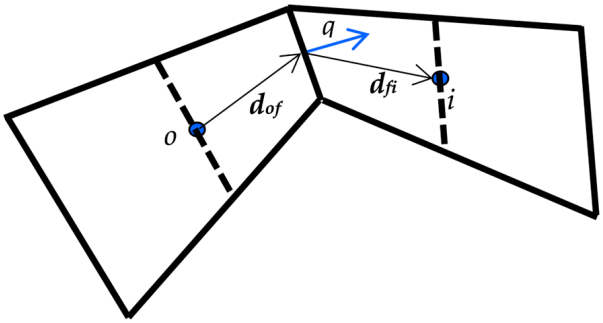


Figure 3. Implied control volume for face velocity delineated by dashed lines.

The momentum equation in mixed vector-tensor notation is

$$\frac{\partial(\varrho \mathbf{u})}{\partial t} = -\nabla(\rho \mathbf{u} \otimes \mathbf{u}) + \nabla\sigma - \nabla p + \mathbf{S} \tag{2}$$

where $\boldsymbol{\sigma}$ is the deviatoric stress tensor that is related to the rate of strain tensor in the usual manner and $\mathbf{S}$ stands for any body force that may be present.

Attention is now focused on the spatial derivative terms in Equation (2), which may be discretised in a finite-volume fashion (by integrations over the control volume V_o invoking the Gauss theorem) for each node (o) to relate $\mathbf{u}_o$ to its surrounding neighbours. The present method is general and applies to any choice of standard difference scheme; hence, there is no need to express the result of the discretisation with reference to any specific difference formula, and it suffices to present it as

$$\int \left[-\nabla \rho \boldsymbol{u} \bigotimes \boldsymbol{u} \right) + \nabla\sigma \Big] dV \Longrightarrow H(\boldsymbol{u}) - A_c^o \boldsymbol{u}_o \tag{3}$$

where

$$H(\boldsymbol{u}) = \sum A_i^o \boldsymbol{u_i} \tag{4}$$

and the summation is over all neighbouring nodes i. The A_i^o coefficients are a result of the discretisation scheme used and the central coefficient A_c^o is generally given by

$$A_c^o = \sum A_i^o \tag{5}$$

Consider the nodal Cartesian velocity vector at node o; the resulting momentum equation for it can be written (ignoring the time derivative term for the moment) as

$$A_c^o \boldsymbol{u}_o = H(\boldsymbol{u}) + \int (\nabla p)_o dV + \boldsymbol{S}_o \tag{6}$$

Now, the cell face velocity $\boldsymbol{u}_f^o$, as seen from node o, can be taken to be

$$\boldsymbol{u}_f^o = \boldsymbol{u}_o + \Delta \boldsymbol{u}_o \tag{7}$$

where $\Delta \boldsymbol{u}_o$ is the difference in the values of the velocity between the node and cell-face; hence, for example, for the u Cartesian velocity component, it is given by

$$\Delta u_o = (\nabla u)_o \cdot \boldsymbol{d}_{of} \tag{8}$$

This technique of incorporating the velocity gradient in the interpolation for the face velocity is very similar to that adopted by Aguerre et al. [23], who albeit continued in that work to pursue a standard collocated scheme.

A similar equation for the v component is formulated. Hence, Equation (6) can be rewritten as

$$A_c^o \boldsymbol{u}_f^o = H_o(\boldsymbol{u}) - A_c^o \Delta \boldsymbol{u}_o + \int (\nabla p)_o dV_o + \boldsymbol{S}_o \tag{9}$$

Now consider the corresponding face velocity $\boldsymbol{u}_f^i$ relating to the node i straddling the same face f; it may be taken as

$$\boldsymbol{u}_f^i = \boldsymbol{u}_i - \Delta \boldsymbol{u}_i \tag{10}$$

The corresponding momentum equation for $\boldsymbol{u}_f^i$ then becomes

$$A_c^i \boldsymbol{u}_f^i = H_i(\boldsymbol{u}) + A_c^i \Delta \boldsymbol{u}_i + \int (\nabla p)_i dV_i + \boldsymbol{S}_i \tag{11}$$

It should be pointed out that accounting for the velocity gradients $\Delta \boldsymbol{u}_i$ is crucial in preventing the occurrence of oscillations in the velocities that could arise on non-uniform or highly distorted meshes.

Finally, the cell face velocity $\mathbf{u}_f$ is taken to be a distance-weighted average of $\boldsymbol{u}_f^o$ and $\boldsymbol{u}_f^i$, given by Equations (9) and (11). Denoting the averaged quantities with an overbar, one obtains

$$\overline{\left(\frac{\rho V}{\delta t} + A_c\right)} \boldsymbol{u}_f = \overline{H(\boldsymbol{u})} + \overline{A_c \Delta \boldsymbol{u}} + \overline{D}(p_i - p_o) + \overline{E(\Delta p)_r} + \overline{\boldsymbol{S}_f} + \overline{\frac{\rho V}{\delta t}} \boldsymbol{u}_f^n \tag{12}$$

where the temporal derivative term has now been included, with the old time-level value denoted by superscript n. The pressure gradient term in Equation (12) has been split into the staggered pressure difference $(p_i - p_o)$ and a "cross-derivative" term $(\Delta p)_r$, which is the remainder of the volume integral of the pressure gradient force. Thus,

$$\overline{(E \Delta P)_r} = \int \left\{ \overline{\nabla p} - \left[\left(\nabla p_{\,o} \cdot \boldsymbol{d}_{of} \right) \boldsymbol{e}_{of} + \left(\nabla p_{\,i} \cdot \boldsymbol{d}_{fi} \right) \boldsymbol{e}_{fi} \right] \right\} dV \tag{13}$$

where $\mathbf{e}_{of}$ and $\mathbf{e}_{fi}$ are the unit vectors along $\mathbf{d}_{of}$ and $\mathbf{d}_{fi}$, respectively.

Quantities D and E in Equation (12) are areas corresponding to the related pressure gradients.

In the validation cases to follow, two methods have been used to compute velocity and pressure gradients, both leading to almost identical solutions. The first was by application of Gauss's theorem. The second was by fitting the grad operator to all nodes within and those surrounding the cell in question; thus, for the u Cartesian component, for example, it may be written as

$$(\nabla \boldsymbol{u})_{\boldsymbol{o}} \cdot (\boldsymbol{d}_{\boldsymbol{of}} + \boldsymbol{d}_{\boldsymbol{fi}}) = u_i - u_o \tag{14}$$

A least-squares method is then used find the components of the gradient operator.

With the values of the Cartesian velocities $\mathbf{u}_f$, the velocity q normal to the cell-face can be determined from Equation (1). With the assembled values of q at all cell faces, the continuity equations (here, incompressible flow is assumed) can be enforced:

$$\sum_f \rho_f q_f a_f = 0 \tag{15}$$

where a_f is the cell-face area.

2.3. Reconstruction of the Nodal Velocities

Several proposals appear in the literature for the reconstruction procedure, this being the scheme for computing the nodal values of velocities from the face values. As far as the present authors know, all the existing techniques derive the nodal values from the face *fluxes* or the velocities *normal* to the faces. This appears to be a reasonable procedure since the fluxes satisfy continuity explicitly. However, from the experience of the present authors, such a procedure has shown to give mixed results, particularly on highly skewed meshes. Here, it is proposed that the nodal Cartesian velocities are better determined directly from the cell-face Cartesian values themselves. In the present work, two procedures have been adopted and are described below; both gave almost identical results.

Scheme A.

Reconstruction is achieved here by simple weighting of the inverse distance from the cell centre to the cell face; thus,

$$\boldsymbol{u}_o = \sum_f w_f \boldsymbol{u}_f \tag{16}$$

where w_f is a weighting factor for each face, given by

$$w_f = \frac{\frac{1}{[\![\boldsymbol{d}_{of}]\!]}}{\sum \frac{1}{[\![\boldsymbol{d}_{of}]\!]}} \tag{17}$$

Different weighing factors may be ascribed to the different velocity components depending on the orientation of the cell face.

Scheme B.

The formula developed by Perot [10] is reinterpreted and applied to the individual Cartesian face-velocity components (rather than the face-normal velocity as used by other methods). Thus, it can be re-cast as

$$\boldsymbol{u}_o V = \sum \left(\boldsymbol{d}_f \cdot \boldsymbol{n}_f \right) a_f \boldsymbol{u}_f \tag{18}$$

However, it was found to be necessary to invoke the velocity gradient corrections proposed by Natarajan & Sotiropoulos [19] as well as give lower weighting to the face velocities that are parallel to the face in some cases.

3. Method of Solution

The above set of equations is simultaneous in the Cartesian components of **u**, the face velocities $\mathbf{u}_f$, and the pressure p. The set may be solved using either (i) an iterative coupled-solution technique, which is most suited to steady-state flow cases, or (ii) a segregated solution method, which can either be iterative or use a predictor–corrector approach, which is most suited to unsteady flows. Here, PISO (Issa [7]) is adapted to solve the set of equations, and it was chosen as a suitable tool to highlight the strong pressure-velocity coupling mechanism afforded by the proposed staggered method. It should be stressed, however, that this chosen method is not a necessary prerequisite for handling the proposed staggered scheme.

The sequence of the solution process follows similar steps to the original PISO scheme and proceeds as follows:

1. In the predictor step, the A coefficients in the momentum in Equations (3) and (5), resulting from the discretisation on the collocated mesh, are assembled.

2. The values of the H operators in Equation (4) are then computed from values of $\mathbf{u}^n$ at the previous time step.
3. The values of $\mathbf{u}_f$ are then computed from Equation (12) using the old pressure field; these are then used to compute the face-normal velocities q_f from Equation (1), whose values do not in general satisfy continuity (unless steady state is reached).
4. A first corrector pressure equation is solved using the face normal velocities just computed.
5. The face velocities are then corrected corresponding to the new pressure field.
6. The nodal velocity components are reconstructed from either Equation (16) or (18), and new velocity gradients as well as corresponding H operators are updated accordingly. New mass fluxes are then calculated.
7. A second pressure equation is then solved for an updated pressure field, which is then used to update the face velocities, followed by a reconstruction step to compute the nodal velocity components.
8. A new time step is initiated.

In the present work, the full stencil pressure equation, including cross-derivatives, is solved in unsteady flow utilising the BICGSTAB [24] technique.

4. Validation

4.1. Preamble

The purpose of the validation cases (in two dimensions) is as follows:

1. To demonstrate the efficacy of the pressure-velocity coupling in hybrid methods of the present sort compared to standard collocated methods, leading to superior solution stability on skew meshes;
2. To show that the present method preserves the order of accuracy of the discretisation scheme on the collocated mesh used (here, second-order centred difference is used);
3. To demonstrate a much superior kinetic energy conservation property to that of collocated methods;
4. To verify the efficacy of the PISO algorithm using two correctors with the proposed scheme on a model case.

It should be stressed that the following comparisons of the performance of the staggered technique against the collocated method are based on identical finite-volume discretisation schemes (centred difference) in both methods. Indeed, the present staggered method was implemented in an existing collocated-scheme code; hence, the comparison is like with like.

4.2. Inviscid Channel Flow

The PISO method was originally developed for meshes that are (i) staggered and (ii) orthogonal. The efficacy of the technique relies on the incorporation of momentum and pressure updates in two corrector steps satisfying continuity and momentum together in an implicit form. However, with the introduction of the collocated mesh methodology using the Rhie & Chow [3] interpolation, the nodal velocities lose their strong connection to the pressure gradients: those gradients that drive the nodal velocity are not the same as those driving the cell face velocities. Reversion to a staggered arrangement, such as the one proposed here, should recover the strong connection between velocity and pressure, and this is verified in this example.

The current case is of a one-dimensional inviscid, incompressible flow in the channel depicted in Figure 4, where there is a sudden change in inlet velocity. The mesh used in the simulation is stretched in both directions, with 44×20 cells, and the results can be compared with an analytic solution.

The velocity along the channel at time $t = 0$ is uniform at 0.1 m/s; then, there is a sudden change at the inlet to 0.5 m/s at the first time step, which is taken arbitrarily as $\delta t = 1$ s. Since the flow is incompressible, the velocity throughout the channel adjusts instantaneously at the first-time step to the inlet value, while the pressure gradient can be computed from the Euler equation as

$$dp/dx = -\rho \delta u/\delta t \tag{19}$$

At the second time step, since the velocity remains uniform at its new inlet value, the pressure gradient becomes zero along the channel.

The computed axial velocity and pressure fields are compared with the analytic solutions in Figures 5–8 for the first two time steps. Simulation using the present staggered method matches the analytic solution after the necessary but sufficient two PISO correctors are performed.

When the same case is tackled with the collocated method, two PISO correctors are entirely insufficient to give the exact solution; hence, more correctors are required, and here it was found that no fewer than 50 correctors were needed to drive down the magnitude of the velocity oscillations and approach the exact solution, as shown in Figures 7 and 8.

Although this case is an academic one, it serves to illustrate the weakness in the handling of pressure–velocity coupling in the collocated scheme. This weakness stems from the fact that the pressure gradients driving the nodal velocities are not equal to those driving the cell face velocities. The results demonstrate why PISO is currently used in collocated methods like an iterative scheme (such as PIMPLE incorporated in the code OpenFoam), which defeats its original purpose.

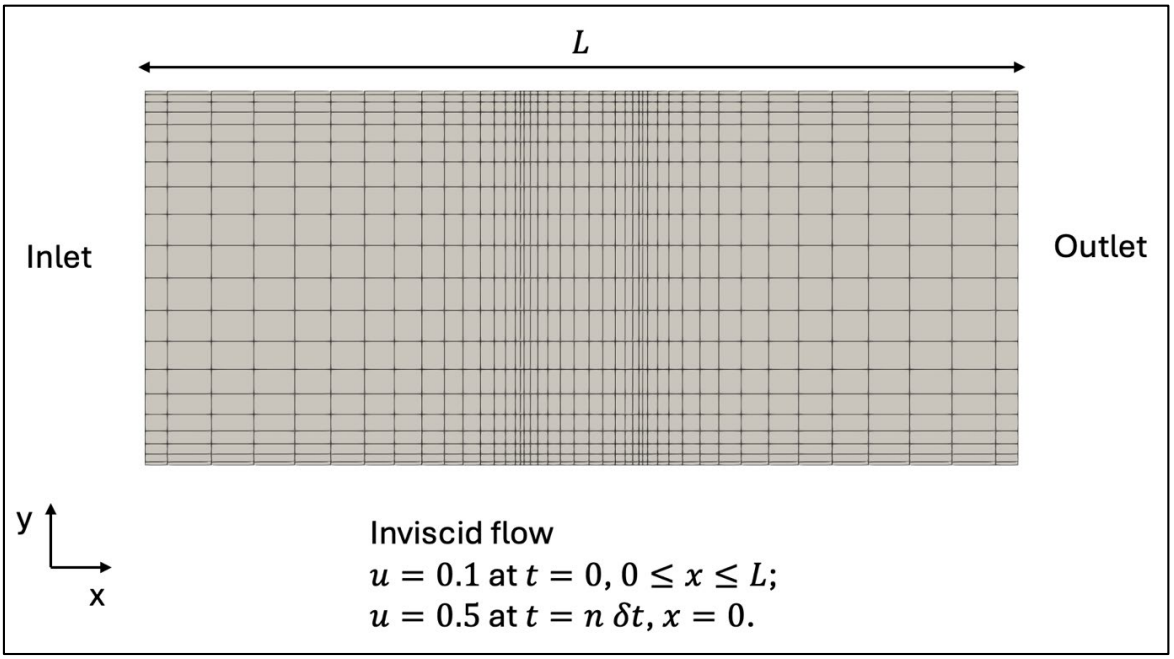


Figure 4. Inviscid flow test case setup.

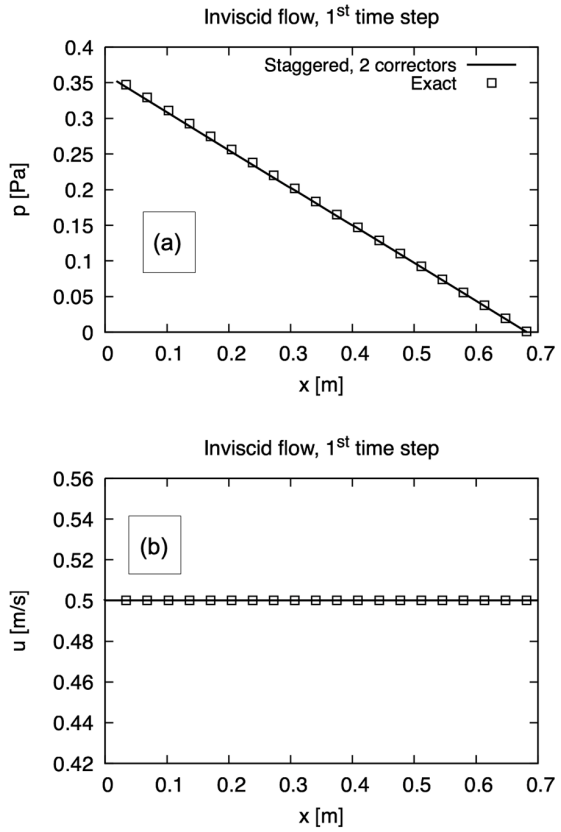


Figure 5. Inviscid flow test case. Pressure (**a**) and velocity (**b**) distributions obtained with the staggered method for the first time step.

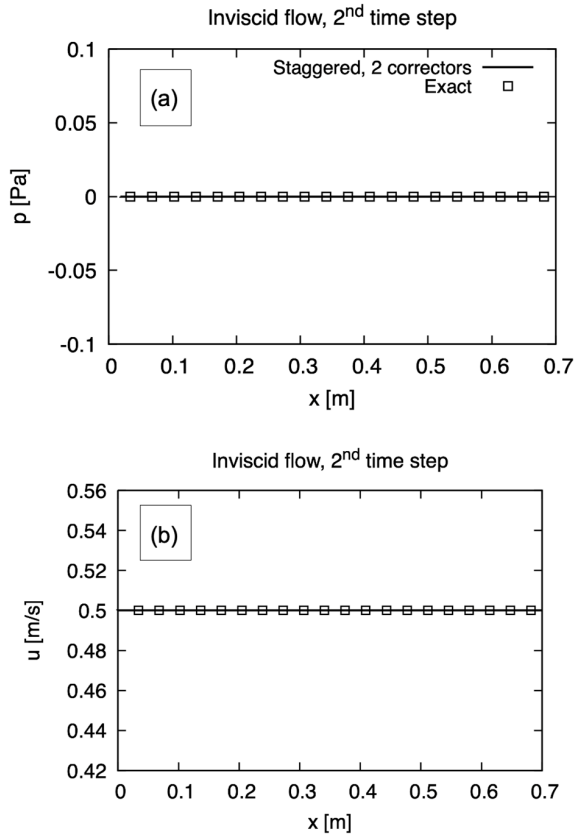


Figure 6. Inviscid flow test case. Pressure (**a**) and velocity (**b**) distributions obtained with the staggered method for the second time step.

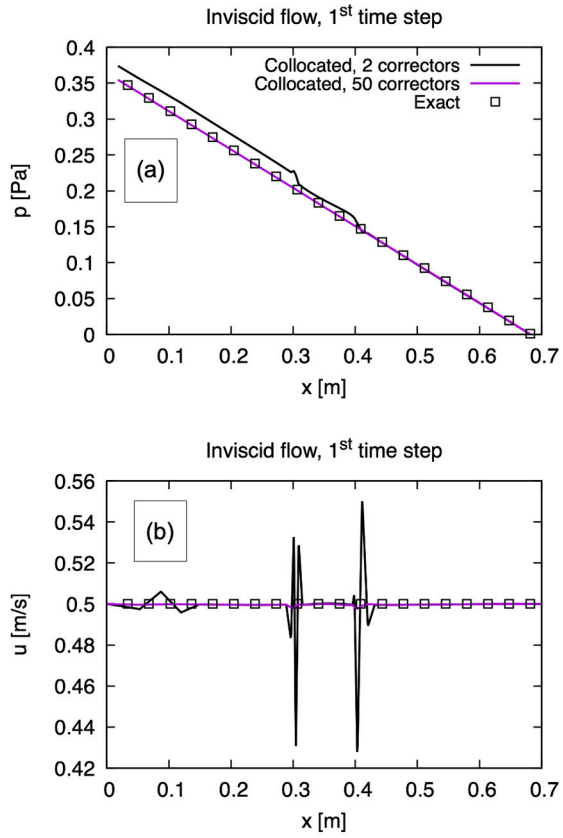


Figure 7. Inviscid flow test case. Pressure (**a**) and velocity (**b**) distributions obtained with the collocated method for the first time step.

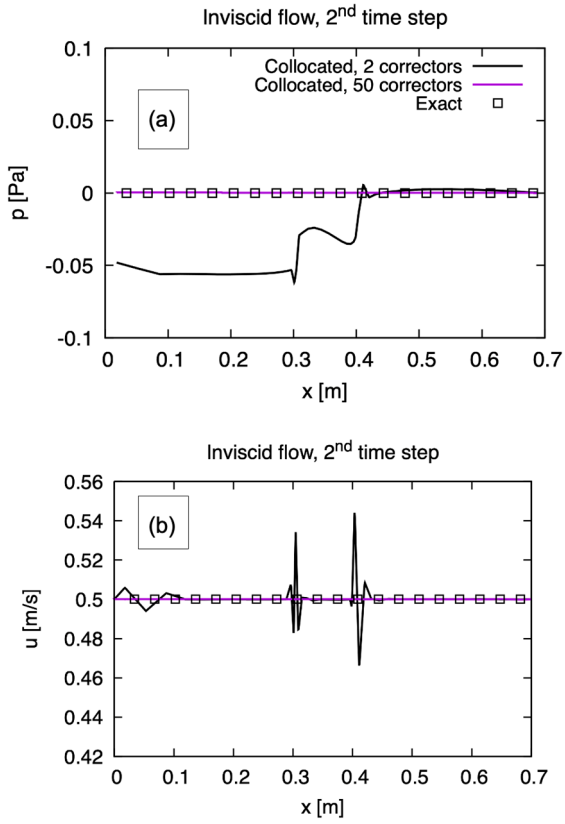


Figure 8. Inviscid flow test case. Pressure (**a**) and velocity (**b**) distributions obtained with the collocated method for the second time step.

4.3. Kinetic Energy Conservation in the Taylor–Green Vortex Flow

This is a classic flow case that is often used to verify the conservation of kinetic energy in the simulation of inviscid flow, where there is no dissipation due to friction. The case is that of counter-rotating vortices, described by

$$u = -sin(x)cos(y) \tag{20}$$

$$v = cos(x)sen(y) \tag{21}$$

where u and v are the Cartesian components of velocity in a square domain of extent $0 \leq x \leq 2\pi$, $0 \leq y \leq 2\pi$.

A mesh of 40×40 cells is used to simulate this case with both staggered and collocated methods. A time step corresponding to a Courant number of 0.1 was used in both cases, for both of which two PISO correctors were used. The velocity patterns for u and v are presented, respectively, in Figures 9 and 10, for the staggered and collocated schemes, after 4000 time steps. It is evident that the staggered scheme preserves the vortex pattern while the collocated one distorts the flow field. The latter scheme was also run with 50 correctors but no significant improvement to the results was obtained.

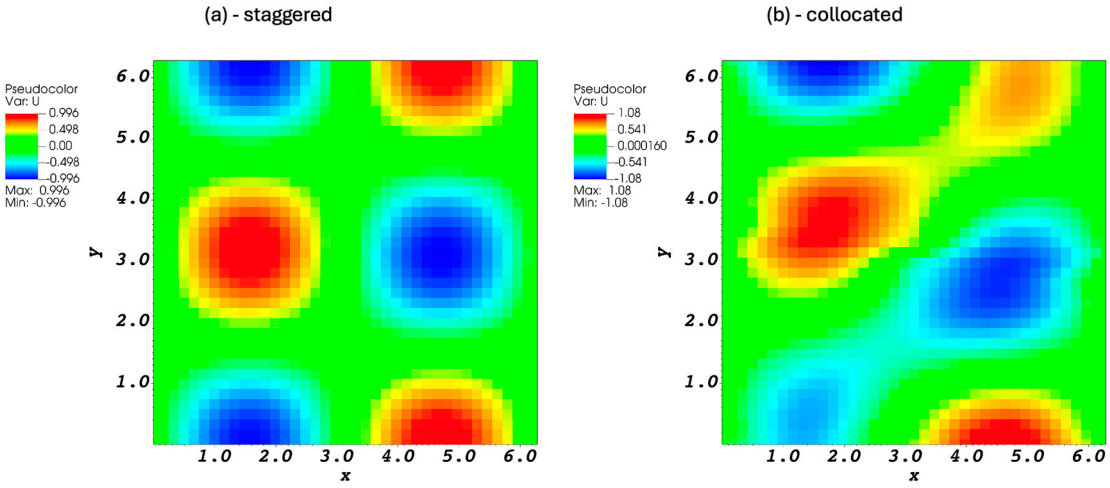


Figure 9. Distribution of u velocity component for the Taylor–Green vortex flow using (**a**) staggered and (**b**) collocated methods.

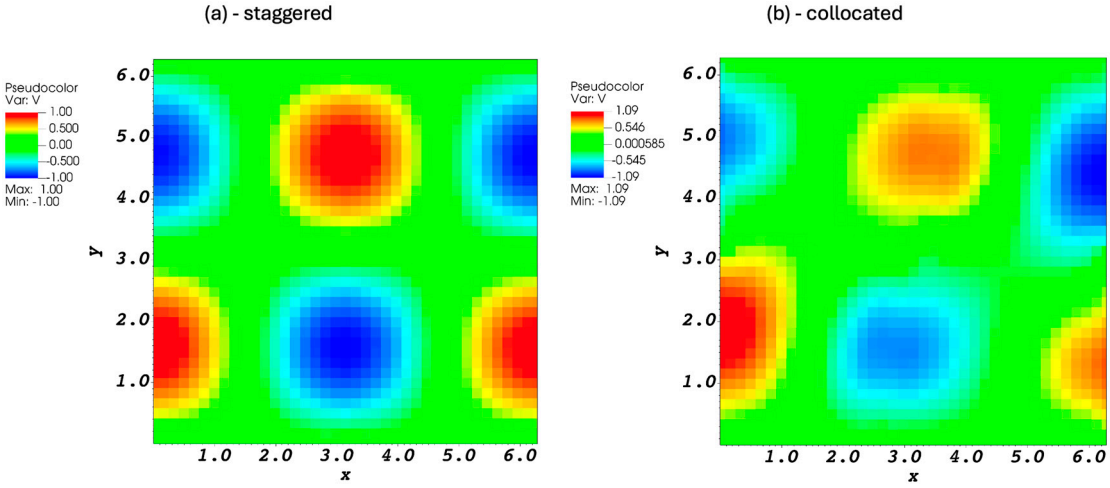


Figure 10. Distribution of v velocity component for the Taylor–Green vortex flow using (**a**) staggered and (**b**) collocated methods.

The kinetic energy in the system, defined by

$$E = \sum \left(u^2 + v^2\right)/2 \tag{22}$$

where the summation is over all the nodal velocities in the domain, is plotted against time as it evolves in the simulation. Its value should be constant since there is no viscous effect, and this is reproduced closely by the proposed staggered scheme, as shown in Figure 11, whereas the collocated method shows a marked depletion in energy as the simulation proceeds, a feature that has been established previously (see, for example, Ref. [5]).

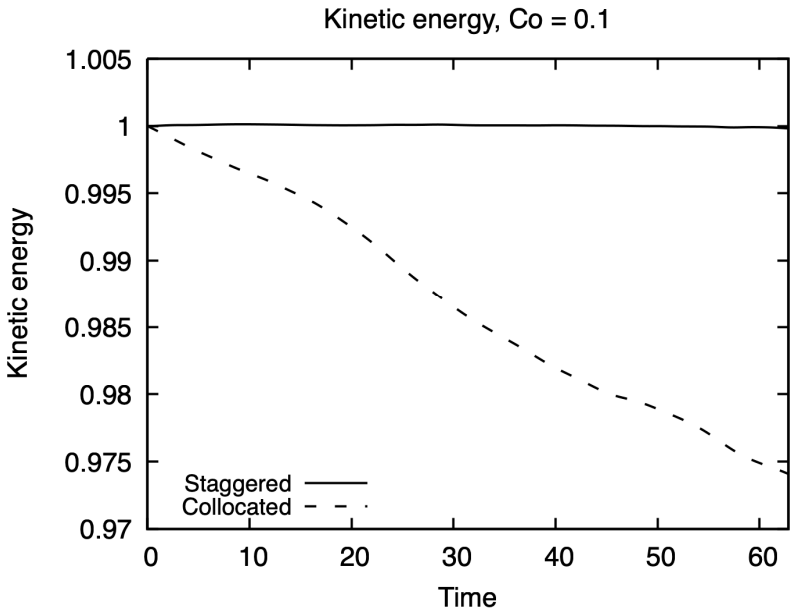


Figure 11. Time history of kinetic energy for the Taylor–Green vortex flow.

The conservation of kinetic energy is naturally linked to the pressure field. For this vortex flow case, an analytical solution for the pressure distribution exists (see, for example, ref. [25]) and is given by

$$p = -\frac{1}{4}\rho(cos(2x) + cos(y2)) \tag{23}$$

and is displayed in the contours of Figure 12. The pressure field obtained from the proposed staggered method at the end of the simulation is shown in Figure 13a, and it clearly matches the analytical solution, whereas the corresponding field predicted by the collocated scheme shows considerable distortion in Figure 13b.

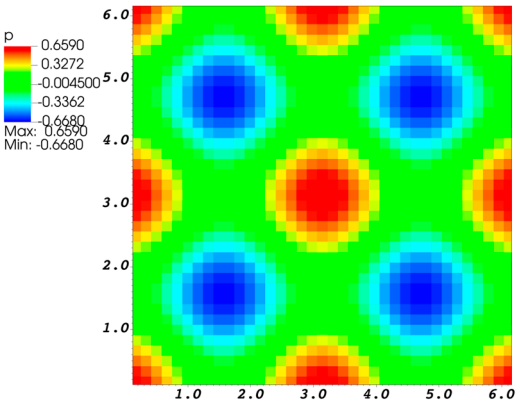


Figure 12. Analytical solution for pressure field in Taylor–Green vortex flow.

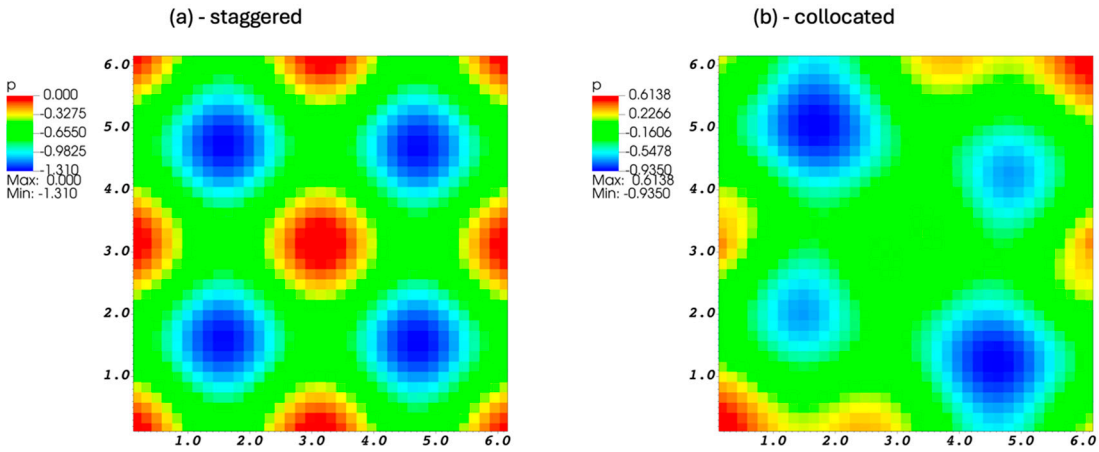


Figure 13. Predicted pressure distribution in Taylor–Green vortex flow using (**a**) staggered and (**b**) collocated methods.

4.4. Lid-Driven Cavity Flow

This is a case that has served as a reference for evaluating various solution methods in the literature. It was presented by Ghia & Ghia [26] who computed with the vorticity-stream function method the two-dimensional viscous flow in a square cavity (of side 1 m), driven by a lid moving along its length, as depicted in Figures 14 and 15, which, respectively, show the predicted streamline patterns for Reynolds numbers of 100 and 1000.

The purpose of the tests here is twofold: (i) to show that on an orthogonal mesh, the present staggered method maintains the same order of accuracy of the differencing scheme used on the cell nodes, and (ii) to show that the new scheme is robust on highly skewed meshes while giving the correct solution at two quite different Reynolds numbers.

4.4.1. Orthogonal Mesh Computations at Re = 100

The results of the computations presented in Figure 16 for the lateral and axial velocity profiles along the mid-lines, on a 160 × 160 uniform mesh, are compared with the reference solutions of Ghia & Ghia. The displayed results collapse on those obtained from the collocated mesh methods embodied in both OpenFoam and the 2D proprietary code mentioned earlier.

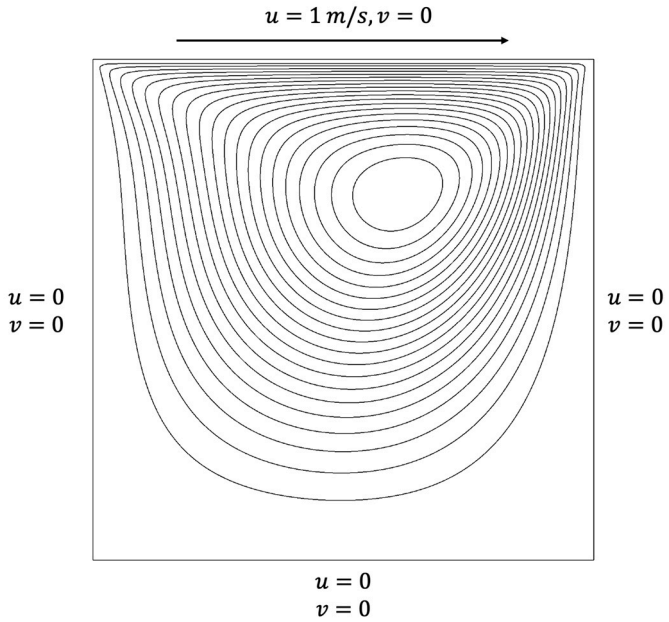


Figure 14. Flow pattern in the lid-driven cavity flow at Re = 100.

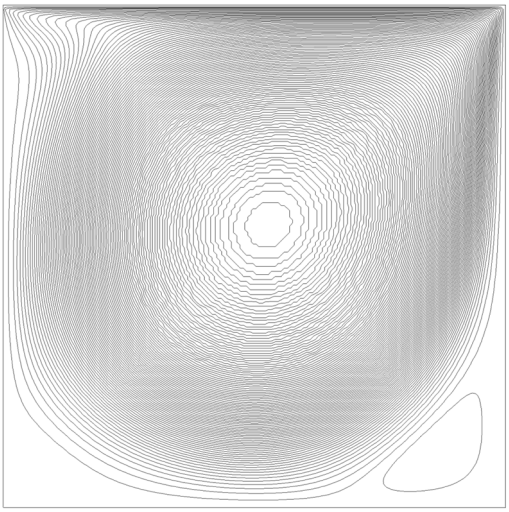


Figure 15. Flow pattern in the lid-driven cavity flow at Re = 1000.

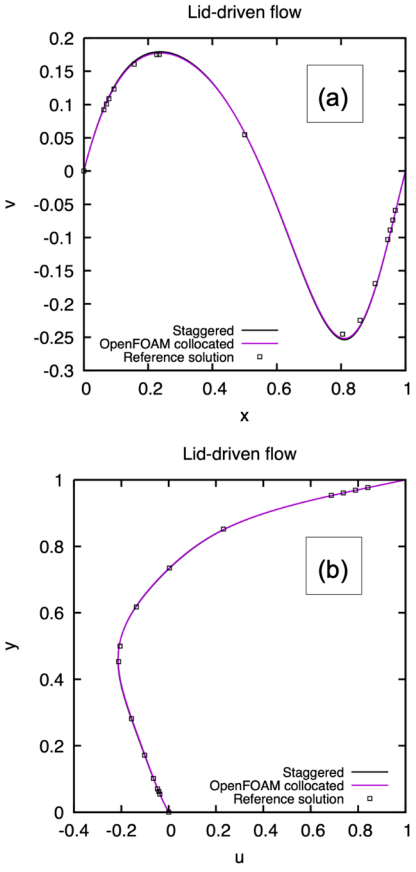


Figure 16. Comparison between midline axial (**a**) and lateral (**b**) velocity profiles of the liddriven flow configuration at Re = 100 obtained with the current method and with a standard collocated approach.

The accuracy of the proposed methodology was tested on a mesh convergence study using uniform meshes, with dx being the cell width, starting with a 20 × 20 mesh and using the solution obtained with a very fine 640 × 640 mesh as the reference solution to calculate a pseudo-error from an average velocity $\overline{u}$, defined as

$$\overline{u} = \sqrt{\frac{\sum(u^2 + v^2)}{V_{tot}}} \tag{24}$$

The total volume (or, strictly, total area, as this is a two-dimensional domain) is V_{tot} and the summation $\sum$ is over all cells in the domain. Since the discretisation of the momentum equations for each cell uses centred-difference, the solution is expected to be second-order accurate on a uniform mesh.

The pseudo-error of a given mesh is computed as

$$\varepsilon = \overline{u}_{mesh} - \overline{u}_{ref} \tag{25}$$

where $\overline{u}_{ref}$ is calculated on the finest 640 × 640 mesh. Figure 17 indicates second-order accuracy via comparison with the solid line corresponding to quadratic error decay.

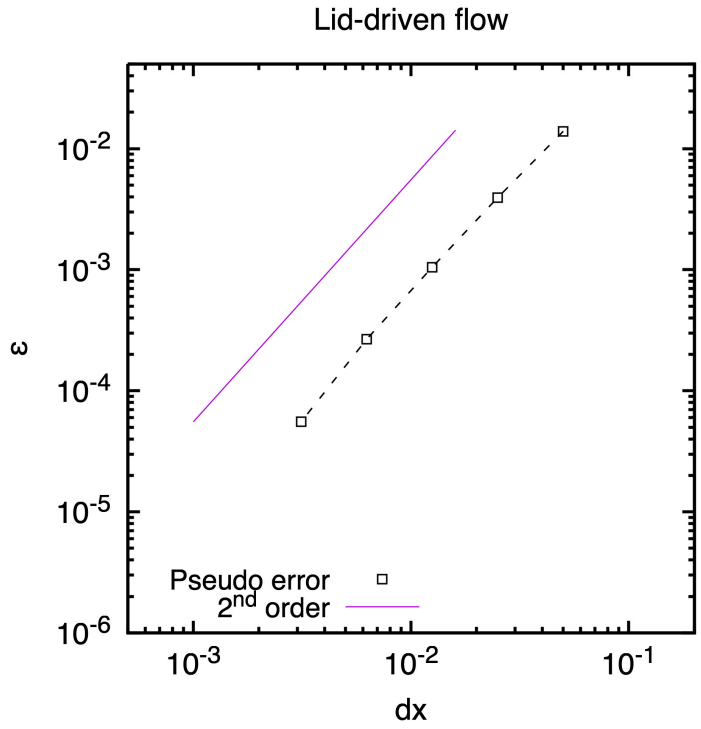


Figure 17. Error decay plot obtained via a mesh convergence study of the Re = 100 lidriven flow case on uniform meshes.

4.4.2. High-Aspect-Ratio Rectangular Meshes at Re = 100

The proposed method, outlined above, was tested to ascertain its applicability and robustness to the modelling of viscous flow on meshes with distorted cells; here, a high-aspect-ratio rectangular mesh was chosen. Initial tests on this mesh without accounting for the velocity gradients given in Equations (7) and (8) resulted in persistent oscillations in the velocity fields. When accounting for those gradients, smooth solutions were obtained as depicted in Figures 18 and 19, which verify the necessity to include those terms.

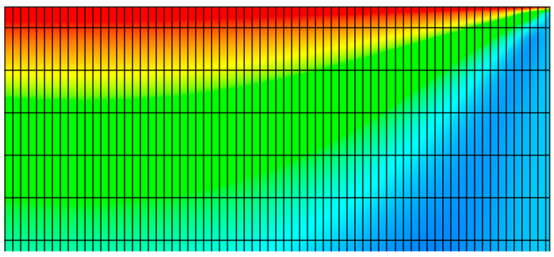


Figure 18. High-aspect-ratio rectangular meshes used in lid-driven flow tests.

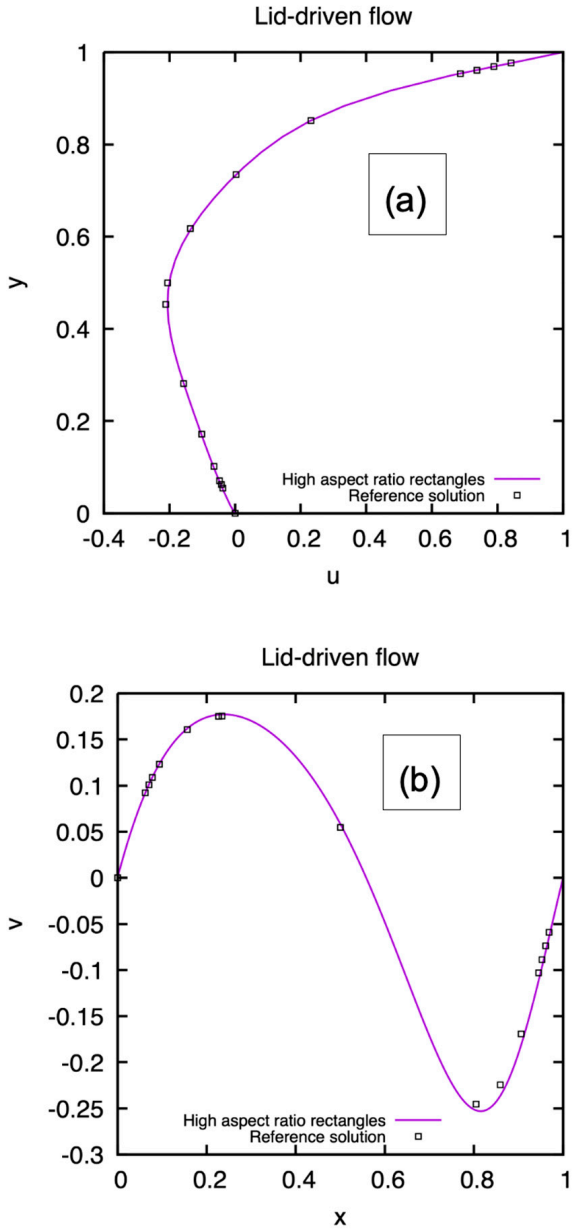


Figure 19. Lateral (**a**) and axial (**b**) velocity profiles obtained with the current method for the Re = 100 lid-driven flow test using high-aspect-ratio rectangular meshes.

4.4.3. Skewed Mesh Computations at Re = 100

A skewed mesh of 159 × 159 cells used for this exercise is one that is stretched from being equilateral on one side of the cavity to almost fully obtuse triangular on the other side. A close-up of the mesh is shown in Figure 20 to illustrate its obtuseness. This mesh proved to be a challenge for various techniques that are proposed elsewhere in the literature. The one presented in this article was successful when reconstruction of the nodal values was based on the averaging of the Cartesian face velocities themselves (as presented earlier) rather than the face fluxes.

The profiles for the axial and lateral velocities presented in Figure 21 again show excellent agreement with both the reference solution and that obtained from the uniform regular mesh.

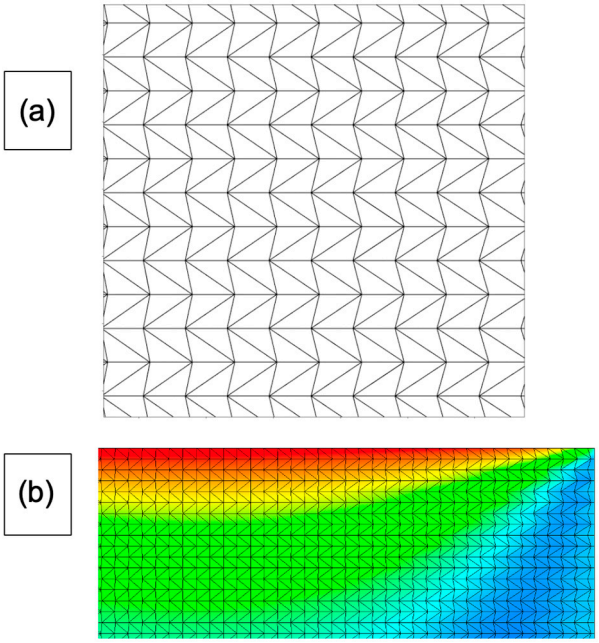


Figure 20. (**a**) Close-up view and (**b**) wider view of the skewed mesh.

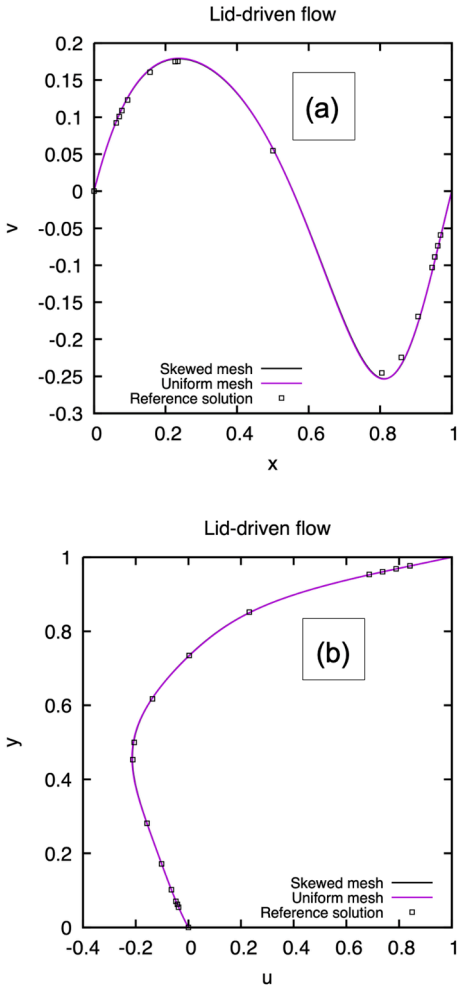


Figure 21. Axial (**a**) and lateral (**b**) velocity profiles obtained with the current method for the Re = 100 lid-driven flow test using uniform and skewed meshes.

For this case of steady-state flow, it is useful to demonstrate the robustness of the staggered scheme versus that of the collocated method on such a skewed mesh. Figures 22 and 23 display the variation in the normalised residuals in the pressure equation with time steps at different Courant numbers for the staggered and collocated methods, respectively. The former clearly shows stability for very high Courant numbers, whereas the latter shows divergence for values of the Courant number well below unity. It is worth noting that the computing time with the collocated scheme at the stable Courant number was 46% higher than that taken by the staggered mesh at the higher Courant numbers (although this may pertain to this particular case). Here, again, it should be noted that both codes used the same parameters and discretisation schemes in obtaining those results.

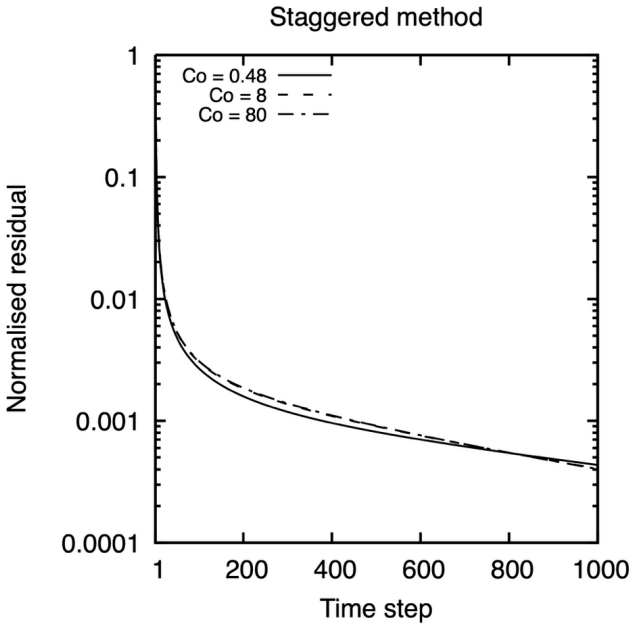


Figure 22. Normalised residuals in the pressure equation for Re = 100 lid-driven flow test using the skewed mesh (Staggered method).

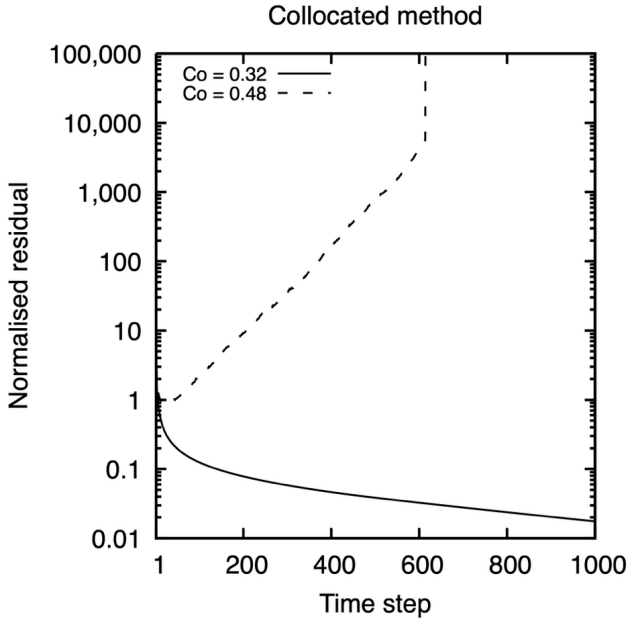


Figure 23. Normalised residuals in the pressure equation for Re = 100 lid-driven flow test using the skewed mesh (Collocated method).

4.4.4. Skewed Mesh Computations at Re = 1000

In order to test the proposed method on a more convection-dominated flow case, the same lid-driven cavity is simulated at a Reynolds number of 1000, for which a reference solution was provided by Ghia and Ghia. The flow pattern in this case is shown earlier in Figure 15. Here, the mesh used is shown in Figure 24, while Figure 25 presents the axial and lateral profiles of the v and u velocity components, respectively.

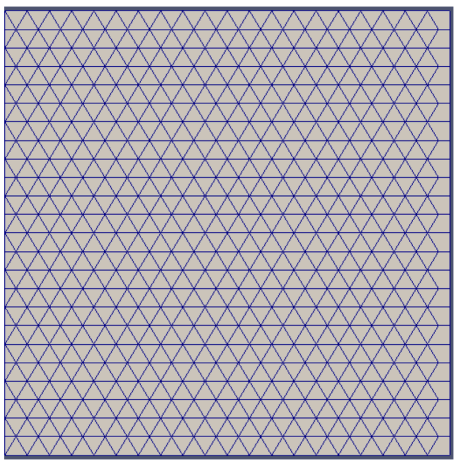


Figure 24. Triangular mesh for the Re = 1000 lid-driven cavity case.

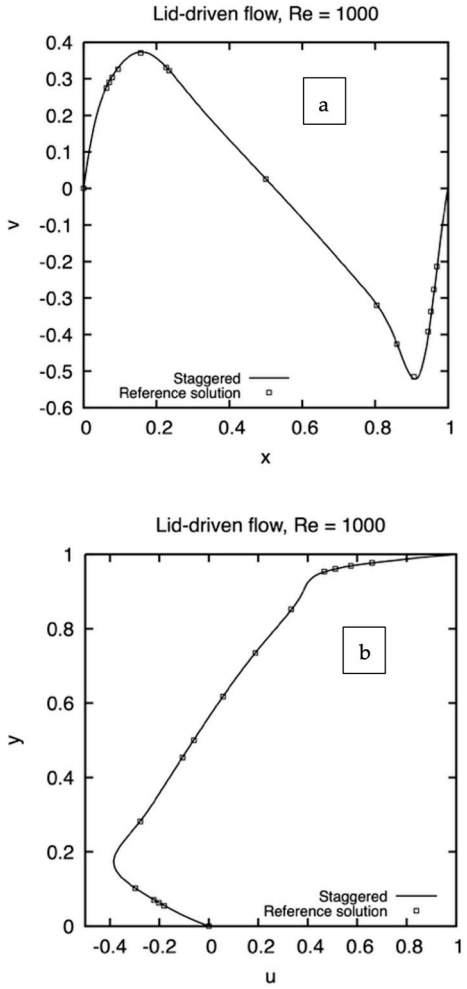


Figure 25. Axial (**a**) and lateral (**b**) velocity profiles obtained with the current method for the Re = 1000 lid-driven cavity flow on skewed mesh.

Here, again, there is excellent agreement between the current predictions and the reference solution.

4.5. Vortex Shedding Flow

The current method was applied to the unsteady flow past a square obstacle studied in [27,28], where regular vortex shedding occurs. Time histories of velocity oscillations downstream of a square obstacle were monitored on both regular and skewed meshes. A sketch of the simulation setup is shown in Figure 26. An example of the skewed mesh configuration is shown in Figure 27.

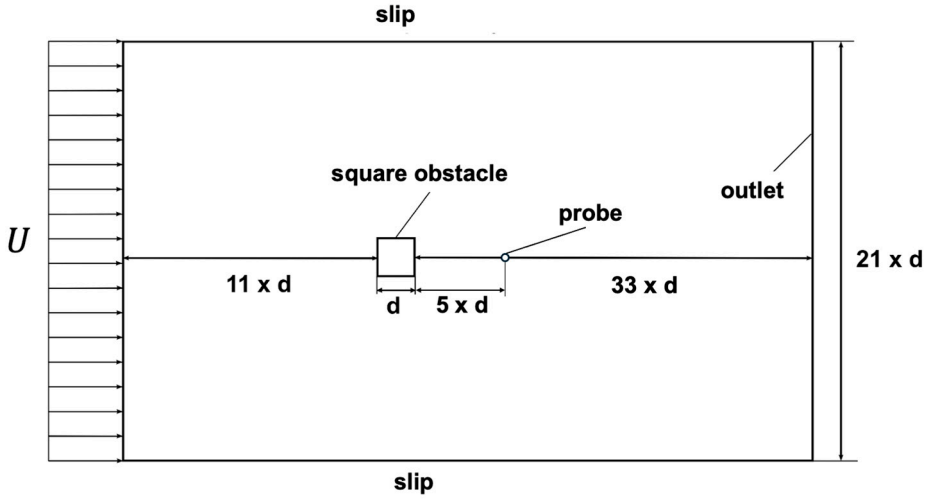


Figure 26. Flow configuration used in the time-dependent flow tests.

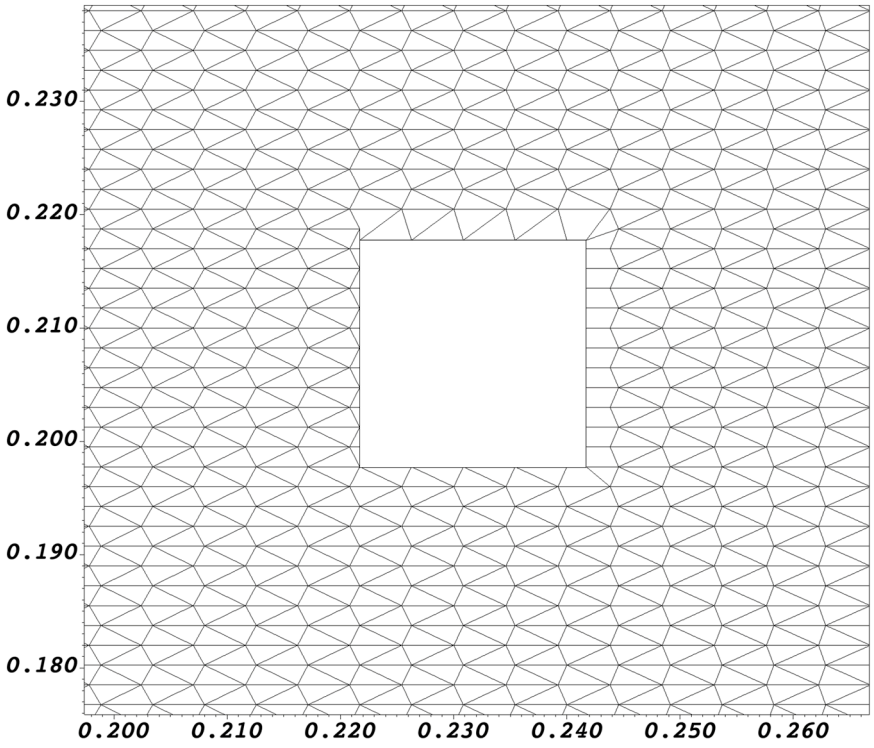


Figure 27. Detail near the obstacle of the skewed mesh used in the time-dependent flow simulations.

The Reynolds number of the flow is 70, which is defined as $Re = \frac{Ud}{\nu}$, where U is the uniform free stream velocity, d is the obstacle side dimension, and ν is the kinematic viscosity of the fluid. The time step of the simulations corresponding to a Courant number

of 0.13 was found to give good temporal accuracy using the Euler time marching scheme. A snapshot of the velocity magnitude field is shown in Figure 28 in the periodic regime during which, as shown in Figure 29, oscillation cycles are stable and characterised by a unique value of the oscillation period T.

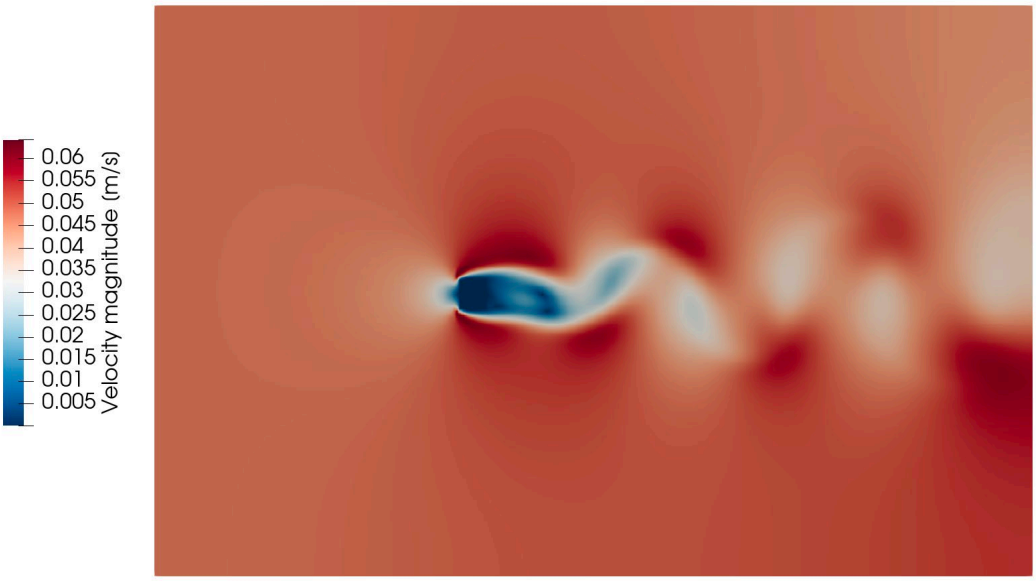


Figure 28. Instantaneous velocity magnitude distribution during quasi-periodic vortex shedding.

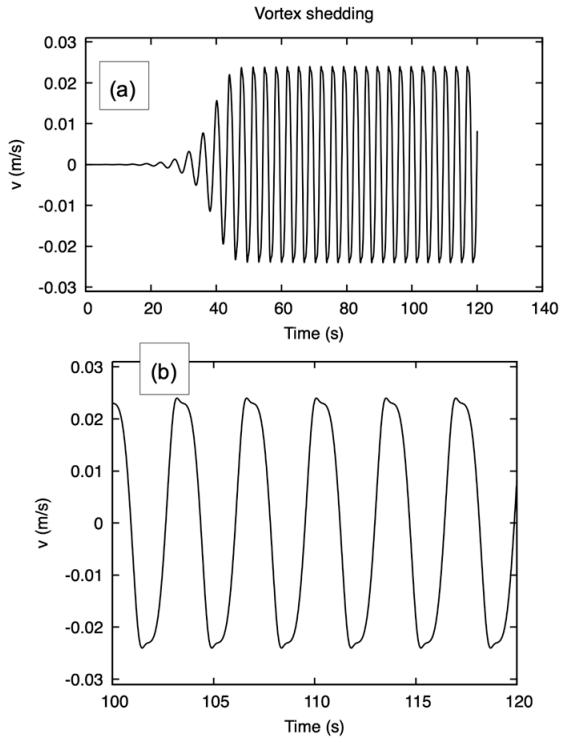


Figure 29. (**a**) Time history of the vertical velocity component v at the monitoring location downstream of obstacle. (**b**) Close-up of the velocity oscillations in the periodic regime.

Simulations with the current method on a uniform mesh consistently indicated a period of $T \simeq 3.42$ s, in agreement with a standard collocated method, as indicated in Figure 30, corresponding to a Strouhal number $St = \frac{d}{UT}$ of approximately 0.12, consistent with the experiments of Refs. [27,28].

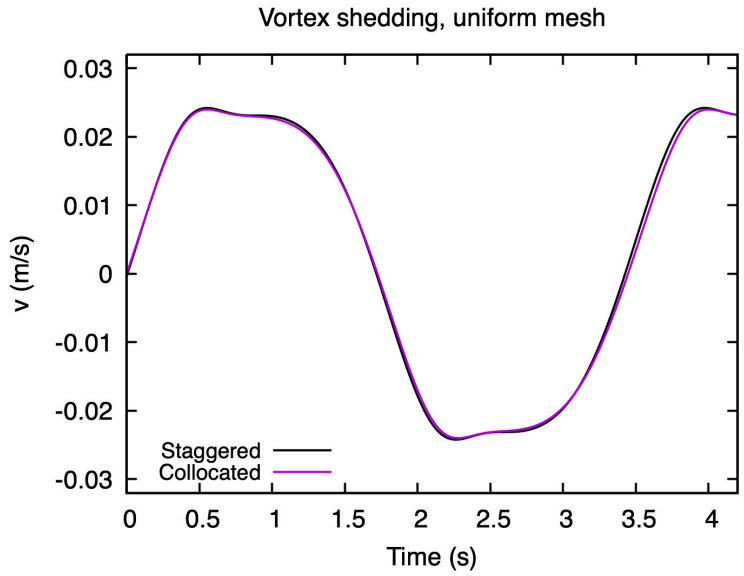


Figure 30. Comparison of time histories of the velocity, during one oscillation period, obtained with the current staggered methodology and with the established collocated methodology.

The application of the method to this case on the skewed mesh shown in Figure 25 yielded results very close to those obtained from the regular uniform mesh, as indicated in Figure 31, thus validating the applicability to highly skewed meshes with little compromise in terms of accuracy.

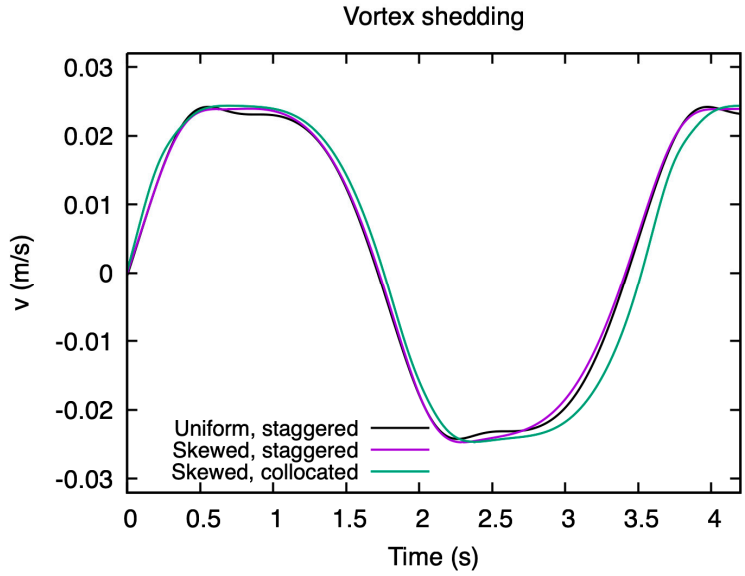


Figure 31. Comparison of time histories of the velocity, during one oscillation period, from simulations on highly skewed meshes using staggered and collocated methods.

However, when the same case on the same skewed mesh was tackled with the standard collocated method, the results (also displayed in Figure 31) were slightly offset from the correct ones, which were obtained with the current hybrid method, although exactly the same discretisation schemes were employed. This inaccuracy in the collocated solution may very well be due to the approximation embodied in the interpolation formula for the face velocities.

5. Conclusions

The performance of a method that combines finite-volume discretisation of the fluid flow equations on a collocated mesh together with a staggered mesh approach is assessed and compared against that of a standard collocated technique. The scheme presented encompasses two aspects that are different from other similar techniques; the first is in the derivation of the momentum equation for the cell-face velocities, and the second is in the way the nodal velocities are reconstructed directly from the face velocities. The former aspect is necessary to prevent the occurrence of oscillatory velocity fields, which had also been pointed out by other workers. The latter aspect is required to ensure accuracy and stability on highly distorted cell configurations.

The validation exercise verifies that the employed technique preserves the order of accuracy of the discretisation on the underlying collocated mesh in viscous flow on uniform meshes while giving accurate results on skewed meshes. It also shows how the PISO methodology recovers its efficacy on the staggered arrangement that was somewhat diminished by collocated mesh methods. Lastly, the tests verify the applicability and accuracy of the technique in unsteady flow on both uniform and skewed meshes.

Future work may be aimed at more general, fully unstructured meshes in three dimensions, including polyhedral ones, as well as the simulation of turbulent flows.

Author Contributions: Conceptualisation, R.I.; methodology, R.I. & G.G.; software, R.I. & G.G.; validation, R.I. & G.G.; formal analysis, R.I. & G.G.; investigation, R.I. & G.G.; resources R.I. & G.G.; data curation, R.I. & G.G.; writing—original draft preparation, R.I. & G.G.; writing—review and editing, R.I. & G.G.; visualization, G.G.; project administration, R.I. & G.G. All authors have read and agreed to the published version of the manuscript.

Funding: This research received no external funding.

Institutional Review Board Statement: Not applicable.

Informed Consent Statement: Not applicable.

Data Availability Statement: The original contributions presented in this study are included in the article. Further inquiries can be directed to the corresponding author.

Conflicts of Interest: The authors declare no conflict of interest.

Nomenclature

Latin letters

a	Cell face area
A	Denotes coefficients of discretised momentum equations
$\boldsymbol{d}$	Distance vectors connecting cell centres to face centres
d	Obstacle side length
D	Coefficient relating to staggered pressure difference
$\boldsymbol{e}$	Unit vector along **d**
E	Coefficient relating to cross-derivative pressure difference
l	Sum of discretised spatial derivatives
L	Length
$\boldsymbol{n}$	Outward unit vector normal to cell face
p	Pressure
q	Velocity component normal to cell face
Re	Reynolds number
S	Body force
St	Strouhal number
t	Time
T	Oscillation period

$\boldsymbol{u}$	Velocity vector
U	Reference velocity
u	Velocity component in x direction
v	Velocity component in y direction
V	Volume
w	Weighting factor
x, y	Cartesian coordinates
Greek symbols	
ε	Pseudo error
ν	Fluid kinematic viscosity
ρ	Fluid density
Subscripts and uperscripts	
c	Denotes central coefficient of discretised momentum equation
f	Denotes cell face
i	Neighbour cell
n	Old time level
O	Cell centre
R	Cross-derivative term
overbar	Distance-weighted average

References

1. Harlow, F.H.; Welch, J.E. Numerical calculation of time-dependent viscous incompressible flow of fluid with free surface. *Phys. Fluids* **1965**, *8*, 2182. [CrossRef]
2. Patankar, S.V.; Spalding, D.B. A calculation procedure for heat, mass and momentum transfer in three-dimensional parabolic flows. *Int. J. Heat Mass Transf.* **1972**, *15*, 1787–1806. [CrossRef]
3. Rhie, C.M.; Chow, W.L. Numerical study of the turbulent flow past an airfoil with trailing edge separation. *AIAA J.* **1983**, *21*, 1525–1532. [CrossRef]
4. Ferziger, J.H.; Perić, M.; Street, R.L. *Computational Methods for Fluid Dynamics*; Springer: New York, NY, USA, 2019.
5. Benhamadouche, S.; Laurence, D. Global kinetic energy conservation with unstructured meshes. *Int. J. Numer. Methods Fluids* **2002**, *40*, 561–571. [CrossRef]
6. Jofre, L.; Lehmkuhl, O.; Ventosa, J.; Trias, F.X.; Oliva, A. Conservation Properties of Unstructured Finite-Volume Mesh Schemes for the Navier-Stokes Equations, Numerical Heat Transfer. *Part B Fundam.* **2014**, *65*, 53–79. [CrossRef]
7. Issa, R.I. Solution of the implicitly discretised fluid flow equations by operator-splitting. *J. Comput. Phys.* **1986**, *62*, 40–65. [CrossRef]
8. Perot, B. Conservation Properties of Unstructured Staggered Mesh Schemes. *J. Comput. Phys.* **2000**, *159*, 58–89. [CrossRef]
9. Perot, B.; Nallapati, R. A moving unstructured staggered mesh method for the simulation of incompressible free-surface flows. *J. Comput. Phys.* **2003**, *184*, 192–214. [CrossRef]
10. Vidović, D.; Segal, A.; Wesseling, P. A superlinearly convergent finite volume method for the incompressible Navier–Stokes equations on staggered unstructured grids. *J. Comput. Phys.* **2004**, *198*, 159–177. [CrossRef]
11. Wenneker, I.; Segal, A.; Wesseling, P. A Mach-uniform unstructured staggered grid method. *Int. J. Numer. Methods Fluids* **2002**, *40*, 1209–1235. [CrossRef]
12. Wenneker, I.; Segal, A.; Wesseling, P. Conservation properties of a new unstructured staggered scheme. *Comput. Fluids* **2003**, *32*, 139–147. [CrossRef]
13. Wesseling, P.; Segal, A.; Kassels, C.G.M.; Bijl, H. Computing flows on general two-dimensional nonsmooth staggered grids. In *Floating, Flowing, Flying: Pieter J. Zandbergen's Life as Innovator, Inspirator and Instigator in Numerical Fluid Dynamics*; Dijkstra, D., Geurts, B.J., JKuerten, G.M., Kuiken, H.K., Eds.; Springer: Dordrecht, The Netherlands, 1998; pp. 21–44.
14. Zijlema, M.; Segal, A.; Wesseling, P. Finite volume computation of incompressible turbulent flows in general co-ordinates on staggered grids. *Int. J. Numer. Methods Fluids* **1995**, *20*, 621–640. [CrossRef]
15. Mahesh, K.; Constantinescu, G.; Moin, P. A numerical method for large-eddy simulation in complex geometries. *J. Comput. Phys.* **2004**, *197*, 215–240. [CrossRef]
16. Ventosa-Molina, J.; Chiva, J.; Lehmkuhl, O.; Muela, J.; Pérez-Segarra, C.D.; Oliva, A. Numerical analysis of conservative unstructured discretisations for low Mach flows. *Int. J. Numer. Methods Fluids* **2017**, *84*, 309–334. [CrossRef]
17. Zhang, X.; Schmidt, D.; Perot, B. Accuracy and Conservation Properties of a Three-Dimensional Unstructured Staggered Mesh Scheme for Fluid Dynamics. *J. Comput. Phys.* **2002**, *175*, 764–791. [CrossRef]

18. Ge, L.; Sotiropoulos, F. A numerical method for solving the 3D unsteady incompressible Navier–Stokes equations in curvilinear domains with complex immersed boundaries. *J. Comput. Phys.* **2007**, *225*, 1782–1809. [CrossRef] [PubMed]
19. Natarajan, G.; Sotiropoulos, F. IDeC(k): A new velocity reconstruction algorithm on arbitrarily polygonal staggered meshes. *J. Comput. Phys.* **2011**, *230*, 6583–6604. [CrossRef]
20. Aguerre, H.J.; Pairetti, C.I.; Venier, C.M.; Damián, S.M.; Nigro, N.M. An oscillation-free flow solver based on flux reconstruction. *J. Comput. Phys.* **2018**, *365*, 135–148. [CrossRef]
21. ANSYS. *FLUENT Release 12.0* ©, ANSYS, Inc.: Canonsburg, PA, USA, 2009.
22. Weller, H.; Shahrokhi, A. Curl-Free Pressure Gradients over Orography in a Solution of the Fully Compressible Euler Equations with Implicit Treatment of Acoustic and Gravity Waves. *Mon. Weather Rev.* **2014**, *142*, 4439–4457. [CrossRef]
23. Aguerre, H.J.; Venier, C.M.; Pairetti, C.I.; Damián, S.M.; Nigro, N.M. A SIMPLE-based algorithm with enhanced velocity corrections: The COMPLEX method. *Comput. Fluids* **2020**, *198*, 104396. [CrossRef]
24. van der Vorst, H.A. Bi-CGSTAB: A Fast and Smoothly Converging Variant of Bi-CG for the Solution of Nonsymmetric Linear Systems. *SIAM J. Sci. Stat. Comput.* **1992**, *13*, 631–644. [CrossRef]
25. Krimi, A.; Ramírez, L.; Khelladi, S.; Navarrina, F.; Deligant, M.; Nogueira, X. Improved δ-SPH Scheme with Automatic and Adaptive Numerical Dissipation. *Water* **2020**, *12*, 2858. [CrossRef]
26. Ghia, U.; Ghia, K.N.; Shin, C.T. High-Re solutions for incompressible flow using the Navier-Stokes equations and a multigrid method. *J. Comput. Phys.* **1982**, *48*, 387–411. [CrossRef]
27. Okajima, A. Strouhal numbers of rectangular cylinders. *J. Fluid Mech.* **1982**, *123*, 379–398. [CrossRef]
28. Luo, S.C.; Tong, X.H.; Khoo, B.C. Transition phenomena in the wake of a square cylinder. *J. Fluids Struct.* **2007**, *23*, 227–248. [CrossRef]

Disclaimer/Publisher's Note: The statements, opinions and data contained in all publications are solely those of the individual author(s) and contributor(s) and not of MDPI and/or the editor(s). MDPI and/or the editor(s) disclaim responsibility for any injury to people or property resulting from any ideas, methods, instructions or products referred to in the content.